JACS
JOURNAL OF THE AMERICAN CHEMICAL SOCIETY

Article

pubs.acs.org/JACS

Patternable Solvent-Processed Thermoplastic Graphite Electrodes

Kevin J. Klunder, Zach Nilsson, Justin B. Sambur, and Charles S. Henry*

Department of Chemistry, Colorado State University, Fort Collins, Colorado 80523, United States

Supporting Information

ABSTRACT: Since their invention in the 1950s, composite carbon electrodes have been employed in a wide variety of applications, ranging from batteries and fuel cells to chemical sensors, because they are easy to make and pattern at millimeter scales. Despite their widespread use, traditional carbon composite electrodes have substandard electrochemistry relative to metallic and glassy carbon electrodes. As a result, there is a critical need for new composite carbon electrodes that are highly electrochemically active, have universal and easy fabrication into complex geometries, are highly conductive, and are low cost. Herein, a new solvent-based method is presented for making low-cost composite graphite electrodes containing a thermoplastic binder. The electrodes, which are termed thermoplastic electrodes (TPEs), are easy to fabricate and pattern, give excellent electrochemical performance, and have high conductivity (700 S m^{-1}). The thermoplastic binder enables the electrodes to be hot embossed, molded, templated, and/or cut with a CO_2 laser into a variety of intricate patterns. Crucially, these electrodes show a marked improvement in peak current, peak separation, and resistance to charge transfer over traditional carbon electrodes. The impact of electrode composition, surface treatment (sanding, polishing, plasma treatment), and graphite source were found to significantly impact fabrication, patterning, conductivity, and electrochemical performance. Under optimized conditions, electrodes generated responses similar to more expensive and difficult to fabricate graphene and highly oriented pyrolytic graphite electrodes. The TPE electrode system reported here provides a new approach for fabricating high performance carbon electrodes with utility in applications ranging from sensing to batteries.

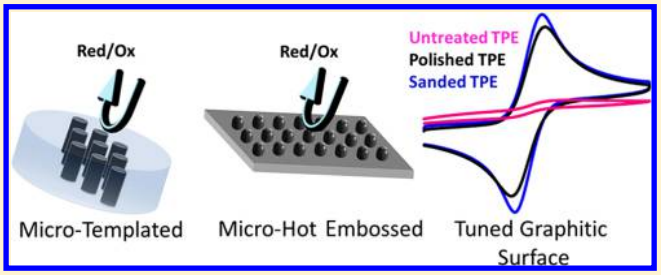

INTRODUCTION

Carbon electrodes have been widely used because of their favorable electroactivity, biocompatibility, chemical stability, high conductivity, wide potential window, and low cost. Common carbon electrodes include glassy carbon, screen-printed carbon (SPE), carbon paste (CPE), boron-doped diamond (BDD), carbon black, pyrolytic graphite, carbon nanotubes, and graphene.[1] The breadth of applications of carbon-based electrodes is diverse and includes batteries,[2] fuel cells,[3] wastewater treatment,[4,5] supercapacitors,[6] anti-static applications,[7] and chemical sensors.[8,9] One challenge with carbon electrodes, however, is the trade-off between ease of fabrication and electrochemical performance. Composite electrodes (CEs) are made from carbon particles held together with a binder and are among the easiest carbon electrodes to make and pattern into millimeter-sized electrodes.[10] Smaller and more complicated CEs are difficult to make. To assemble carbon CEs, a broad range of binders including wax,[11] ionic liquids,[12] epoxy,[13] and plastics such as poly(methyl methacrylate) (PMMA),[14−16] Teflon,[17,18] and polyethylene[19−21] have been used. While carbon CEs are easy to fabricate, they generally suffer from low conductivity and slow electron-transfer kinetics. As a result, there remains significant interest in developing CEs that are inexpensive and easy to fabricate but also highly conductive and possess high electrochemical performance.

Among binder materials, PMMA has been largely ignored, and only a handful of reports exist on its use as a binding medium. The lack of use of PMMA as a binder is odd considering its low cost, ready availability, solubility in a variety of solvents, and popular use in analytical devices.[22] Methacrylate thermoplastic CEs are known[23] but have largely relied on either complex fabrication methods[14,15] or methods that limit patterning.[24] More recently, an *in situ* polymerization method for making PMMA:carbon nanotube electrochemical devices was developed,[16,25] as well as an impregnation technique to fabricate PMMA:graphite electrodes.[26] While these reports provide a basis for the current studies, it is generally unclear how CEs processing change to parameters such as surface treatment, particle size, carbon source, and binder:carbon composition can be used to improve electrode fabrication, patterning, conductivity, and electrochemical performance.

Here, a new solvent-assisted fabrication technique for generating electrodes we refer to as thermoplastic electrodes (TPEs) is reported. TPEs can be patterned via template printing, embossing, and laser cutting into a variety complex geometries, including flow channel and pillar arrays with micrometer-sized features. Electrode conductivities 10- to 100-fold higher than those of traditional screen-printed carbon

Received: June 21, 2017
Published: August 10, 2017

DOI: 10.1021/jacs.7b06173
J. Am. Chem. Soc. 2017, 139, 12623−12631

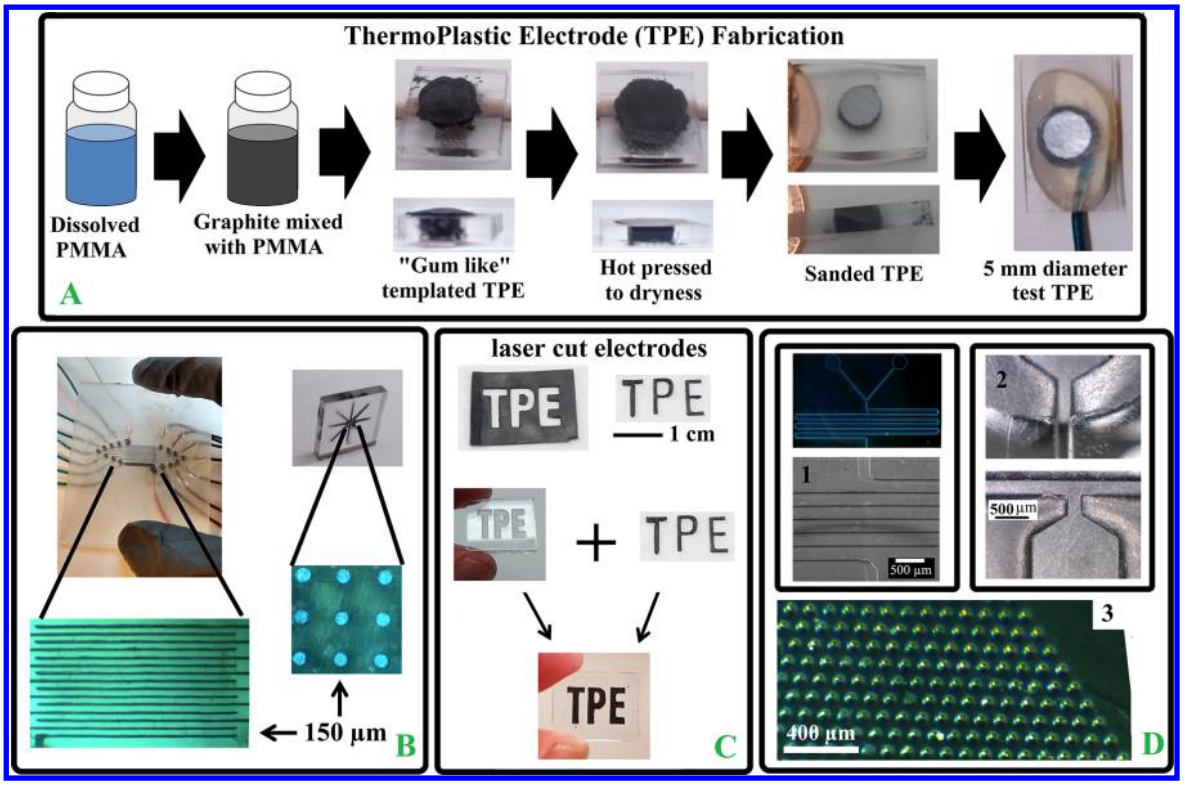

Figure 1. (A) General fabrication method for making templated TPEs. (B) 1:2, 11 μm TPE with 14 individually addressable 150 μm wide bands, and an array of 150 μm diameter individually addressable TPEs. (C) Laser-cut TPE letters, which were hot pressed into a premade matching template. (D1) Serpentine microchannel SU-8 template (top) and the negative embossed image into a 1:0.3, ≤500 nm TPE. (D2) channels embossed in a 1:2, 11 μm TPE. (D3) Hot embossed pillar array using a 1:0.3, ≤500 nm TPE.

electrodes can be achieved by varying the PMMA:carbon ratio, with 11 μm graphite particles giving conductivity as high as 700 S m^{-1}. Following conductivity measurements, electrochemical characterization using cyclic voltammetry and electrochemical impedance spectroscopy in comparison to glassy carbon, screen-printed carbon, and Pt electrodes was carried out using ferricyanide as the redox probe. The TPE outperformed both commercial carbon electrodes and performed similarly to the Pt electrode. A variety of inner- and outer-sphere redox probes designed to test different electron-transfer processes were then evaluated. Surface treatments, including polishing, sanding, and plasma exposure, provide the ability to tune the reactivity, activating and deactivating the electrode for certain chemical systems. Remarkably, with surface treatments, the TPE demonstrates electrochemistry toward the highly surface-sensitive redox probes of dopamine and ascorbic acid comparable to that of the more difficult to prepare electrode materials of graphene, carbon nanotubes, and/or highly oriented pyrolytic graphite (HOPG). Finally, the electrodes were characterized through scanning electron microscopy (SEM) and Raman spectroscopy to elucidate changes in the electrode composition resulting from the surface treatments. Major structural changes of the TPE surface are seen in the SEM images for each treatment. Interestingly, the Raman spectra suggest that the quantity of edge-type defects (crystallite domain size) did not drastically change, with little or no vacancy or sp^3 defects being introduced upon surface treatment. Overall, TPEs provide a significant stepping stone for future advancement in the fabrication and integration of composite carbon electrodes into high-end electrochemical systems.

MATERIALS AND METHODS

Reagents. Poly(methyl methacrylate) (PMMA) was Optix from Plaskolite, and was used as the TPE binder and the template material. Carbon sources were synthetic graphite powder (7−11 μm, 99%. Alfa Aesar), acetylene carbon black (100% compressed, STREM Chemicals), synthetic graphite powder (<20 μm, Sigma-Aldrich), and carbon nanopowder (≤500 nm, 99.95% trace metal basis, Sigma-Aldrich). Chemicals were potassium ferricyanide (99%, Sigma-Aldrich), potassium phosphate monobasic (99.8%, Sigma-Aldrich), potassium phosphate dibasic (98%, EMD Chemicals), potassium chloride (99−100.5%, Sigma-Aldrich), hexaammineruthenium(III) chloride (Sigma-Aldrich), ascorbic acid (99%, Sigma-Aldrich), dopamine hydrochloride (Sigma-Aldrich), iron(III) nitrate nonahydrate (Fisher), and 1,2-dichloroethane (Fisher).

Conductivity Measurements. Through-plane resistivity (inverse of conductivity) was measured by a two-point probe (Fluke 187 multimeter, accuracy of 0.01 Ω) placed on opposing faces of a TPE cylinder, with typical cylinder dimensions on the order of ∼3 mm thick and a diameter of 2−5 mm. Further details on measuring conductivity can be found in the Supporting Information (SI).

Electrochemical Measurements and Surface Treatment. Electrochemistry was performed with a CHI 660 potentiostat, using a saturated calomel electrode (SCE) reference saturated with KCl. The counter electrode was a 1:3 PMMA:carbon TPE plate made using 20 μm particles with an area that exceeded that of the working electrode by at least 10-fold. Potassium ferricyanide solutions were 10 mM, using a 0.5 M KCl solution. Impedance measurements were done at the $E^{1/2}$ of the ferricyanide redox couple taken from cyclic voltammetry at 100 mV s^{-1}; the perturbation voltage was 10 mV, with a frequency range from 100 000 to 0.1 Hz. Dopamine, ascorbic acid, and iron nitrate solutions were made in 0.1 M phosphate buffer at pH 7.4. Hexaammineruthenium(III) chloride experiments were at 1 mM in a 0.5 M KCl solution. The platinum electrode had a diameter of 1.8 mm, TPE electrodes were 5 mm in diameter, glassy carbon was 3 mm in

DOI: 10.1021/jacs.7b06173
J. Am. Chem. Soc. 2017, 139, 12623−12631

diameter, and the DropSens electrode was 4 mm in diameter. The surface treatments were plasma exposure (after sanding) for 3 min at 35 W in ambient air, wet sanding (firm pressure) with 600 grit paper, and wet polishing with a micro-fiber pad with 0.05 μm alumina for ~1 min with firm pressure.

Capacitance Measurements. The capacitance was measured with cyclic voltammetry using the current response at 0.2 V vs SCE, with a totaled sampled region of −0.1 to 0.5 V vs SCE, and a scan rate of 100 mV s^{-1}. Example voltammograms can be found in Figure S4. Averaged capacitance from cyclic voltammetry was calculated using eq 1,

$$C_{area} = \left(\frac{|I_{anodic}| + |I_{cathodic}|}{(2V)A} \right) \quad (1)$$

where C_{area} is the geometric area-normalized capacitance, V is the scan rate (V s^{-1}), $I_{anodic} + I_{cathodic}$ is the width of the cyclic voltammogram at 0.2 V vs SCE, and A is the area of the electrode.[27]

Spectroscopy. A JEOL JSM-6500F field emission scanning electron microscope was used at a 15 keV accelerating voltage to capture images. Raman spectroscopy was performed on an Olympus IX-73 optical microscope with an Ondax THz-Raman laser source (5 mW, 532 nm laser with a 1.2 μm spot size). The Raman signal was collected in a backscattering geometry, passed through a Horiba iHR-550 imaging spectrometer, and detected on a Synapse back-illuminated deep depletion charge-coupled device (CCD). Individual spectra were acquired for 60 s across a 1 mm × 1 mm sample area. The crystallite domain size was calculated using eq 2,

$$L_a\ (\text{nm}) = (2.4 \times 10^{-10})\lambda_l^4 \left(\frac{I_D}{I_G} \right)^{-1} \quad (2)$$

where L_a is the domain size in nm, λ_l is the wavelength of the laser, and (I_D/I_G) is the ratio of the peak intensity of the D and G bands.

RESULTS AND DISCUSSION

Fabrication, Templating, and Patterning of Thermoplastic Electrodes (TPEs). To address the key problem of ease of fabrication and templating, we report a simple and low-cost solvent-assisted fabrication method as an alternative to air-free *in situ* synthetic conditions commonly used with PMMA.[16] Templating TPEs to make complex electrode geometries is straightforward, as illustrated in Figure 1A. Applying pressure (~50 psi) to the TPE while drying was found to be crucial to achieve a defect-free and uniform electrode material. The gum-like consistency of the partially dried TPE material allowed for easy fabrication of electrodes with micrometer-scale dimensions. The ~150 μm spot size of the CO_2 laser used to cut the templates defined the lower size limit of attainable features within the PMMA templates. Figure 1B shows a 150 μm band electrode array, as well as an individually addressable disk electrode array containing 150 μm electrodes. Either electrode array would be challenging to fabricate with traditional carbon materials but can be readily fabricated with the solvent-assisted TPE system. For patterning based on cutting methods, 1−2 mm thick TPE sheets were made by pouring the mixture into a small mold. Once fully dried, the TPE sheets were cut to create electrodes with complex geometric shapes (Figure 1C). The CO_2 laser TPE cutouts, when heated above the T_g (~121 °C from Plaskolite) with applied pressure (~50 psi), were readily moldable into premade PMMA templates.

Despite the high graphite mass loading in the TPE, it was envisioned that embossing could be used to create intricate patterns with the TPE material. Figure 1D shows structures embossed directly into the TPE, including microfluidic channels and a pillar microarray. Structures like the pillar array are particularly attractive for applications where high electrode surface areas are needed.[28,29] At low carbon content for all particle sizes, the TPE retains PMMA-like character and is easily embossed, while at a higher carbon content, the TPE cannot be shaped into micrometer-sized features due to the reduced PMMA binder content. We found a rough upper limit for carbon content to generate well-resolved embossed features to be 1:2 (PMMA:carbon) for the 11 and 20 μm particles, and 1:0.6 for ≤500 nm particles. The ≤500 nm particles were the most versatile for embossing intricate features, perhaps owing to the small particle size which potentially allowed for facile rearrangement of the carbon polymer matrix. The difference in quality of embossed features can be seen in Figure 1D1 and D2, where the 1:2, 11 μm TPE has rounded edges but the ≤500 nm TPE has nearly perfect edges. It should be noted that the embossing parameters were not optimized, and this initial embossing work represents a starting point for more in-depth studies.

Conductivity Measurements. High electrode conductivity is critical to minimize ohmic drop and improve electrochemical performance. Figure 2 shows a comparison of conductivity as a function of electrode composition. As expected, conductivity increased with increasing carbon content. The conductivity of the ≤500 nm TPEs did not reach saturation and was limited by physical electrode integrity. The trend was also observed for the carbon black particles (50 nm). The conductivity of the 11 μm TPEs increased initially but then decreased at higher loadings. The decrease may be due to particle agglomeration at higher mass loadings, which could limit the number of conductive pathways. A similar conductivity trend was previously observed for a carbon nanotube/graphite/epoxy composite.[30] Similar to the 11 μm particles, the conductivity of the 20 μm TPE increases until reaching a saturation point at a 1:3 PMMA:carbon ratio. The conductivities in Figure 2 are consistent with the literature on carbon composites with similar carbon mass loadings, while the values of the 11 μm TPEs are considered high.[30−32] A recent report on a graphene screen-printed electrode proposed an "extremely high" conductivity of 11.2

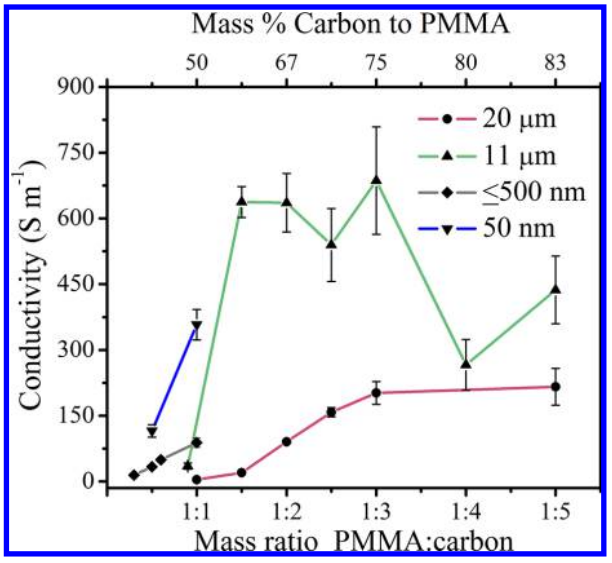

Figure 2. Conductivity as a function of various ratios of PMMA:carbon with differing particle type and size (n = 3). The 20 μm, 11 μm, and ≤500 nm particles were graphitized carbon, and the 50 nm particles were acetylene carbon black.

DOI: 10.1021/jacs.7b06173
J. Am. Chem. Soc. 2017, 139, 12623−12631

S m^{-1}.[8] By comparison, the best-performing 11 μm TPE reported herein exhibited an average conductivity of nearly 700 S m^{-1}.

The high conductivity of TPEs arises most likely from increased numbers of low-resistance particle-to-particle contacts.[33] The contact resistance (quality of contact) between particles, as well as the number of contact points, determines the conductivity of composite materials. In the proposed TPE system, the contact quality and number of contacts will invariably be affected by the particle size, processing technique (pressure), particle shape, and polymer−particle wettability.[33−38] Therefore, given the complexity of the TPE system, the relationship between electrode composition and the exact mechanism that governs a low or a high conductivity is not completely clear. It is clear, however, that the particle source has a profound effect on the resulting conductivity.

Besides providing conductivity information, the data in Figure 2 can also be used to define upper and lower PMMA:carbon mass loading thresholds that allow for a usable electrode. Here, the low carbon mass loading range is defined by a conductivity of 10 S m^{-1}; below this threshold, significant contributions to ohmic drop are observed in an electrochemical cell. The upper limit of mass loading is defined by the mechanical instability of the electrode caused by lack of binder. Figure 2 is also useful for defining the minimum carbon loading required to achieve the maximum electrode conductivity. Higher binder content typically yields electrodes that are more robust and easier to emboss, which have a lower capacitance. Constructing plots like Figure 2 is then quite valuable when optimizing TPE composition for a given application

Electrochemical Characterization of TPEs. Initially, the capacitance of various TPE compositions was quantified, as it is a major contributor to background signal that negatively affects the sensitivity and detection limits in sensing measurements. Cyclic voltammetry and electrochemical impedance spectroscopy (EIS) were used with a variety of redox probes to inform on the electrocatalytic activity of the electrodes. Redox probes were chosen to understand the impact of surface treatment (polishing, sanding with 600 grit paper, and plasma exposure) on the electrochemical properties of the TPEs. As proposed by McCreery (Figure S2), species such ferricyanide, ascorbic acid, dopamine, and Fe^{2+}/Fe^{3+} have electrochemical responses which are heavily dependent on the chemistry of the electrode surface (Figure S2).[39−41] The 11 μm particles in a PMMA:carbon ratio of 1:2 are highlighted in the main text due to their favorable embossing characteristics, high conductivity, electrochemical stability, and lower capacitance. Similar data for TPEs fabricated with 1:3, 20 μm and 1:0.55, ≤500 nm particles can be found in the SI.

Capacitance. Electric double layer (EDL) values of TPEs were calculated from cyclic voltammetry (Figure S4) in 0.5 M KCl. Capacitance increases with carbon content for all electrodes and was higher than for common planar electrodes (Figure 3). Typical capacitance values for planar metal (platinum, gold) electrodes are 20 μF cm^{-2}, for glassy carbon electrodes are 24−36 μF cm^{-2}, and for basal and edge plane graphitic carbon electrodes are ≤2 and ∼60 μF cm^{-2}, respectively.[1] The 2−20 times increased capacitance for many of the 11 and 20 μm TPEs above planar edge or basal graphite points toward an electrode with some surface roughness, especially in the higher carbon-to-PMMA ratios. The dependence of capacitance on graphite content is highlighted with the

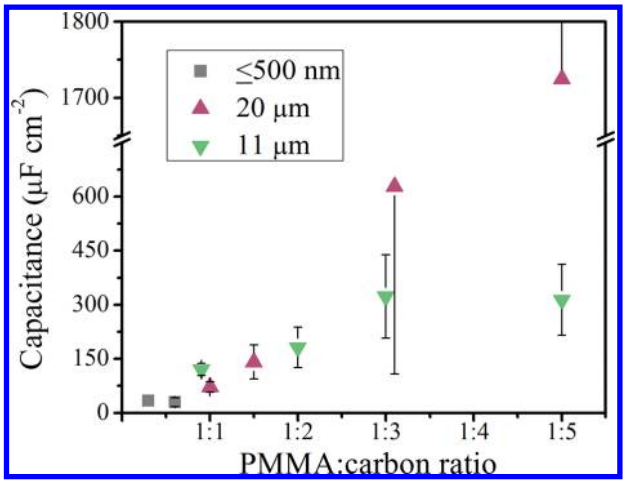

Figure 3. Geometric area normalized capacitance as a function of PMMA:carbon mass loading and particle size with sanded electrode surfaces. For clarity; a break was placed in the *Y*-axis, causing truncated error bars for the 20 μm data. Error bars are calculated from a single capacitance measurement from three separate electrodes.

1:5 PMMA:carbon TPE using 20 μm particles, where a break in the axis is needed to clearly present all the data. The ≤500 nm TPE had capacitance of 35 ± 15 μF cm^{-2}, which is more consistent with a planar carbon electrode, and similar to the average capacitance of 37 μF cm^{-2} of the tested DropSens commercial screen-printed carbon electrodes. Lastly, Figure 3 shows data for the sanded treatment. In general, it was found that the surface treatments did not significantly affect the capacitance (Figure S4); however, the untreated electrodes had a lower capacitance (∼8 μF cm^{-2}), most likely from plastic binder coating some graphite particles. The surface deactivation of the untreated electrode is consistent with data presented in the following sections.

Comparison to Commercial Electrodes. A comparative study of TPEs to commercially available carbon and Pt electrodes was performed using cyclic voltammetry and EIS (Figure 4). Ferricyanide was used because it is surface sensitive and a popular molecule for initial electrode characterization.[1] DropSens CPE have been reported to have a more favorable electroactivity compared with other commercially available composite electrodes and make for a suitable comparison to TPEs.[42] The cyclic voltammograms show peak separations of 140, 90, 400, and 110 mV for glassy carbon, Pt, screen-printed carbon, and TPE electrodes, respectively. The 10 mM concentration and 500 mV s^{-1} scan rate induce high current densities, which can be difficult for an electrode to meet. However, using these conditions the TPE had a peak current of 500 μA cm^{-2}, close to the ideal peak current density (510 μA cm^{-2}) as calculated from the Randles−Sevcik equation (SI, eq S3), and the highest of all electrodes tested. It is noteworthy that the peak separation with the TPE is more like glassy carbon and platinum, most likely from the intrinsic high conductivity. Peak separation is often used for extracting kinetic information, however, in this instance cell resistance/ohmic drop cannot be ruled out as a contributing factor to peak separation. Therefore, EIS was used to gain insight into electrode kinetics as it can decouple cell resistance/ohmic drop from charge transfer resistance.

In Figure 4B the TPEs with surface treatments are compared with screen-printed carbon, Pt, and GC electrodes. The spectra are shown in decreasing charge transfer resistance (diameter of

DOI: 10.1021/jacs.7b06173
J. Am. Chem. Soc. 2017, 139, 12623−12631

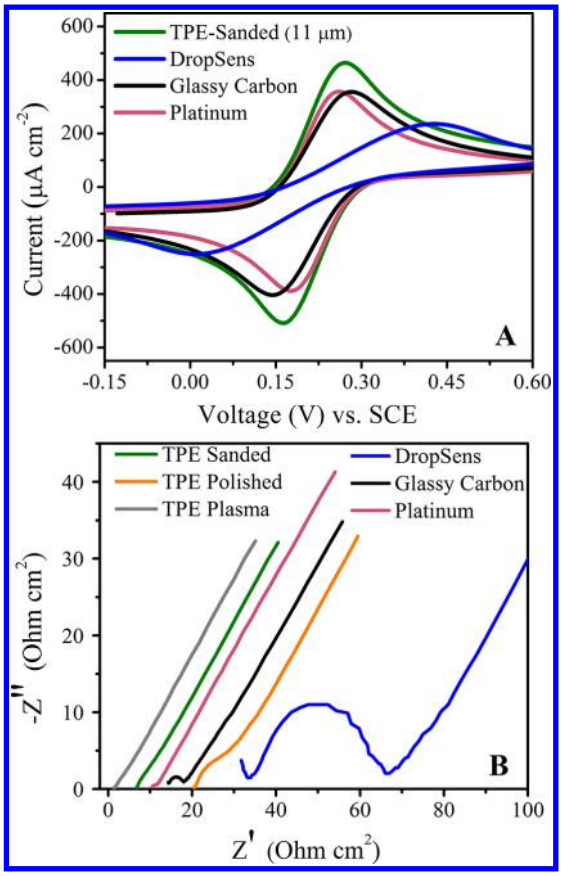

Figure 4. (A) Cyclic voltammetry of a 1:2, 11 μm sanded TPE, Pt, GC, and DropSens electrodes with potassium ferricyanide redox couple (10 mM), scan rate was 500 mV s^{-1}. (B) Impedance spectra (Nyquist plot) taken directly after the cyclic voltammograms. Note, the spectra are manually shifted on the x-axis for clarity.

semicircle) with the spectra manually shifted on the x-axis for clarity. The impedance spectra for the sanded and plasma treated TPEs have no discernible charge transfer resistance. Under these conditions, TPEs appear to be kinetically similar to Pt as well as seemingly outperforming glassy carbon and screen-printed carbon. Attempts were made to sand and plasma treat the screen-printed carbon electrode similar to the TPE treatments, but in both cases electrode performance did not improve (data not shown). Interestingly, polishing the TPE had a detrimental effect on its charge transfer resistance, seen as a larger partial semicircle in the Nyquist plot. The SEM images in the following section show that graphite particles are significantly rearranged with polishing and may give a clue into the origin of the higher charge transfer resistance.

Finally, the stability of the TPEs was tested over the course of 3 days with ferricyanide using the simplest surface treatment (sanded). The electrodes were tested, rinsed with Millipore water, then left in ambient air. The cyclic voltammograms in Figure S3 show a 14% and 1% loss of peak current after the first day, which is unchanged on day 3, for the 11 and 20 μm TPEs, respectively. Through cycling and aging both the 11 and 20 μm particles saw nearly a 10 mV increase in peak separation. In contrast, the $\leq$500 nm TPE saw a 30% and 50% decrease in peak current after the first and second days, with nearly a 200 mV increase in peak separation after 3 days of aging. It seems likely that the freshly sanded/cleaved surface of the TPE is picking up contamination slowly from the ambient conditions, and the mechanism is heavily dependent on the particles used in the TPE. Similar fouling was seen on freshly cleaved HOPG under ultra pure conditions.[43]

Surface-Insensitive Probe. $Ru(NH_3)_6^{2+/3+}$ was used to establish Nerstian voltammetric responses from the TPE and to gauge the non-surface-reliant activity of the electrode (Figure 5A). $Ru(NH_3)_6^{2+/3+}$ is well known to be insensitive to the

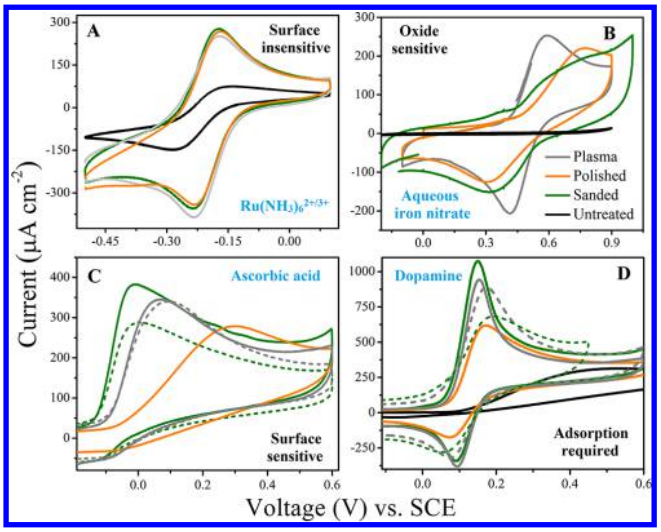

Figure 5. Cyclic voltammograms of a 1:2, 11 μm TPE with $Ru(NH_3)_6^{2+/3+}$, 1 mM ascorbic acid (AA), 1 mM dopamine (DA) in 0.1 M phosphate buffer at pH 7.4. The electrolyte for $Ru(NH_3)_6^{2+/3+}$ was 0.5 M KCl. Dashed lines represent cyclic voltammograms after the electrode has been cycled in the respective solution for 25 cycles.

electronic and/or chemical structure of the electrode surface and has been used to calculate electrochemically active surface area.[44] It was observed that untreated TPEs, for three separate electrodes, gave a lower current density (140 $\pm$ 50 μA cm^{-2}) than theoretically predicted (240 μA cm^{-2}), suggesting surface deactivation. Interestingly, the untreated electrode appears to display microelectrode behavior, evident from the quasi sigmoidal shape of the voltammogram, most likely arising from "active islands" of graphite. Microelectrode behavior is a well-known characteristic of some composite electrodes.[45] When TPEs are sanded, polished, or plasma treated, the electrochemical activity is substantially higher. At a 100 mV s^{-1} scan rate, peak separation for the TPEs are close to Nerstian at 61 $\pm$ 2 mV (three separate electrodes). Since the peak currents are close to theoretically predicted, massive amounts of nano- or microscopic porosity are not expected with the chosen TPE composition. Sponge like porosity can cause an increase in peak current in a cyclic voltammogram from thin layer effects within the porous electrode material, which can be problematic with electrochemical characterization of small carbon particles like carbon nanotubes, graphene, and, potentially, composite electrodes.[46,47] Importantly, while the 1:2, 11 μm TPE does have increased surface roughness shown from capacitance measurements, it does not appear that the electrode has excessive sponge-like porosity with all surface treatments.

Oxide-Sensitive Probe. The $Fe^{2+/3+}$ redox couple is known to be highly sensitive to surface carbon oxides.[39] The cyclic voltammograms in Figure 5B show a drastic difference in peak separation with the various surface treatments. After plasma exposure, the TPEs exhibit well-defined reversible peaks, implying the addition of quinone functionality. The peak

DOI: 10.1021/jacs.7b06173
J. Am. Chem. Soc. 2017, 139, 12623−12631

separation for a plasma treated surface is 150 mV, which is comparable to an electrochemically heavily oxidized highly oriented pyrolytic graphite (HOPG) electrode.[41] Sanded and polished surfaces have peak separations nearing 400 mV, more akin with GC electrodes polished under ambient conditions. Plasma generation of oxides on graphite is well known and is most likely the cause of the peak separation decrease.[48] Oxygen groups generated from milling or sheering in the fabrication of the micrometer-sized carbon particles could explain the partial activity of the sanded and polished electrodes toward $Fe^{2+/3+}$.[49] It can thus be concluded that the graphite most likely contains quinone functionalities with all surface treatments, with plasma treatment yielding the highest population of oxygen moieties on the carbon surface.

Surface-Sensitive Probe. The oxidation of ascorbic acid (AA) is an irreversible two electron, two proton process, that is highly surface sensitive.[50] The electrochemical oxidation of AA can be problematic and numerous electrode modifications have been proposed to enhance electrode kinetics.[51,52] The voltammetry of AA at TPEs (Figure 5C) appeared to have no pre-concentration effects, in agreement with predicted responses (Figure S2), and aligned relatively well with predicted peak currents. Calculation of theoretical peak current (343 $\mu A\ cm^{-2}$) requires a different equation than the previously used Randles–Sevcik equation as detailed in the SI (eq S2). The polished electrode gave a lower peak current and a ~400 mV positive shift in the peak potential, demonstrating the extreme surface sensitivity of AA oxidation. The average onset potential of a sanded single TPE (repeated six times) was -0.032 ± 0.008 V vs SCE, which is similar to or better than that of electrodes composed of carbon nanotubes or graphene,[53,54] and lower than edge plane HOPG (0.2 V vs SCE).[55,56] With the sanded TPE, the peak does not shift to higher potentials with repetitive cycling, although the peak current decreases by 26% after 25 cycles. The peak current for the plasma-treated TPE had excellent stability and remained essentially constant through repetitive cycling. One explanation for the stability may be from the introduction of additional oxygen moieties on the plasma-treated TPE, which have been shown to give an enhanced and stable electrochemical response for AA, DA, and uric acid.[57] Figure S5 contains cyclic voltammograms for TPEs with 20 μm and the ≤500 nm particles with AA. The TPEs with 20 μm particles had voltammetry similar to that of the 11 μm particle TPE, while the ≤500 nm particles-based TPE typically had lower peak currents and increased overpotentials with sanding and polishing conditions. Lastly, the reproducibility of the 11 μm TPE was examined with AA; representative data are shown in Figure S6. For two separate TPEs, repeatedly sanded (n = 6), peak current RSDs of 5.1% and 8.0% were observed. The RSD of peak current across 8 individual electrodes was 15.4%. In addition, the oxidative peak location was quite sensitive to sanding with an average across all eight electrodes of -0.023 ± 0.016 V vs SCE.

Surface Adsorption Dependence. The electrochemistry of dopamine is known to vary on different types of graphitic surfaces. For example with HOPG, there are accounts of low activity on the basal plane compared to edge plane sites.[58] It is also known that the cleanliness of the surface and preparation of basal plane HOPG greatly affects the voltammetry of dopamine.[59] Figure 5D shows the peak locations are in general agreement for clean graphitic surfaces, with the oxidative peak current occurring at 0.147 ± 0.007 V vs SCE (eight separate electrodes/sanded treatment).[59] It was found that the peak currents with TPEs and dopamine do not follow the Randls–Sevick equation for a two-electron oxidation (490 $\mu A\ cm^{-2}$). The observed current was closer to a four electron process, arising most likely from dopamine pre-concentration (adsorption) on the surface as seen for other composites.[60] Similar trends were observed for 20 μm and ≤500 nm TPEs (Figure S5). Dopamine fouling (at 1 mM) is reportedly different for edge plane and basal plane graphite. For HOPG, the oxidation peak potential shifts only slightly with edge plane fouling, while the peak current is reduced to roughly 50%, before becoming relatively stable.[59] With TPEs, the fouling appears to be edge-plane dominated for sanded and plasma-treated electrodes. Remarkably, the peak current and peak location for plasma treated electrodes at 1 mM remains stable with cycling. Similar to the cycling stability of AA, the enhanced stability toward DA may be related to an increase in oxygen functionalities.[57]

The reproducibility of the 11 μm electrodes was tested with the same conditions as in Figure 5 using DA. For three individual TPEs, which were each repetitively sanded (n = 6) to expose a fresh surface, the RSDs for oxidative peak current were 6.0%, 4.7%, and 11.7%, for an average of 7.5%. The RSD for oxidative peak current across eight different individual TPEs was 11.8%, implying that reproducibly is dominated by the surface treatment. The oxidative peak location had an RSD of 4.5% for the eight individual TPEs, and an average RSD of 1.7% for three individual electrodes repetitively sanded. Unlike AA the reproducibility of DA in terms of peak location seems more favorable across different electrodes with a standard deviation of 0.007 vs 0.016 V for DA and AA, respectively. Overall, considering the highly surface sensitive nature of DA and AA, the general reproducibility of TPEs is promising.

TPE Surface Treatment and Characterization. *SEM Characterization of TPEs.* The electrochemistry of TPEs is profoundly affected by surface treatment. SEM and Raman spectroscopy were used to gain insight into structural or chemical changes following the surface treatments. The SEM images in Figure 6 show a significant difference in the TPE surface as a function of treatment method. First, the untreated surfaces (top left) appear to be coated with a polymer film. The lack of charging implies that the polymer film is thin, given that

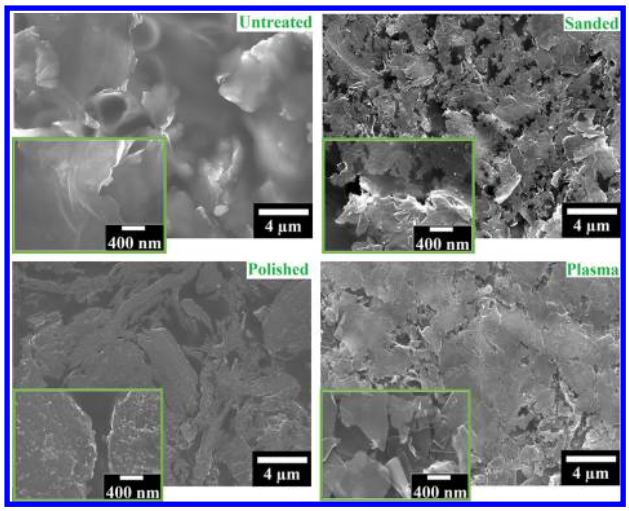

Figure 6. SEM images at 5000× of a 1:2, 11 μm TPE subjected to the various surface treatments. The insets are at 50000× magnification of the surface.

DOI: 10.1021/jacs.7b06173
J. Am. Chem. Soc. 2017, 139, 12623–12631

electrons can efficiently migrate to conductive networks in the TPE during imaging. Second, relative to the untreated electrode, the sanded electrode (top right) has large jagged domains of exposed graphite. The sanded surface is highly complex and undoubtedly contains a myriad of unique carbon chemical environments, including edge planes, ideal for facilitating electrochemical charge transfer. Third, the polished TPE (bottom left) has a drastically altered surface containing clumps or islands where individual graphite sheets are almost unobservable, which may explain the significantly diminished electrochemical response. Finally, the plasma treated electrode (bottom right) is seemingly devoid of polymer binder on the surface, and the removal of binder has exposed thin (semitransparent) sheets of graphite (inset). One hypothesis as to the origin of the thin graphite sheets is that sheer force from sanding is exfoliating the graphite. Excess PMMA is then removed from the exfoliated graphite via the plasma treatment, which ultimately creates graphene-like regions on the TPE surface. Sheer force has been reported to produce high quality graphene in large quantities.[61] Additionally, the plasma-treated and sanded 11 μm electrodes are strikingly similar to a graphene film mechanically pressed onto a plastic substrate.[62] TPEs made with the 20 μm particles had morphologies similar to the 11 μm particles for the respective surface treatments (Figure S7). The $\leq$500 nm TPE was void of the appearance of graphitic sheets and had small, uniform ~100 nm features, as well as having much less morphological diversity than the 11 μm electrodes as a function of electrode treatment (Figure S8).

Raman Characterization of TPE. Finally, the TPEs were characterized with Raman spectroscopy to observe chemical changes which could impact electrochemical performance (Figures 7 and S9). The spectra in Figure 7 represent the

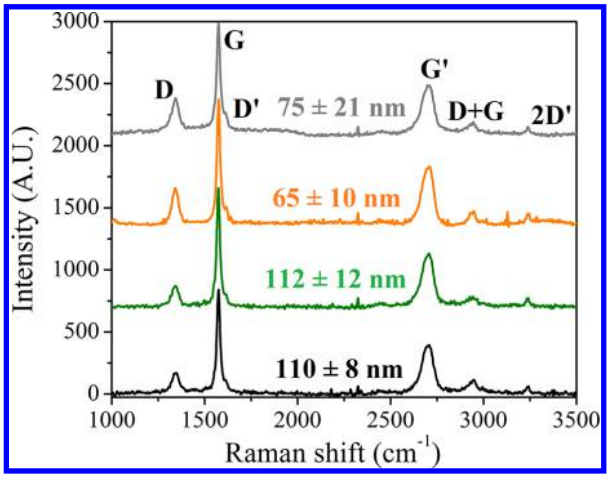

Figure 7. Raman spectra of a 1:2, 11 μm TPE subjected to various surface treatments. Graphite crystallite domain sizes are listed above each spectrum and calculated from eq 2 taken from the data in Table S1.

average of 49 individual spectra. For all treatments, peaks associated with polycrystalline sp^2 carbon are clearly present (Lorentzian peak fitting results are shown in Table S1).[63] Although mechanical exfoliation of the graphite via sanding or polishing might shift the G' peak position toward lower wavenumber from thinning the graphite sheets, no significant peak shifting between different surface treatments was seen.[64] Additionally, changes in the number of sp^3 defects from treatments would increase the width of the D and G peaks, which was also not observed.[65] Considering mechanical abrasion, plasma treatment, and sheer are known to introduce defects and drastically change graphite composition, it seems unlikely that these processes are not happening in some amount at the TPE surface.[66−68] The lack of changes seen in the spectra are perhaps from the Raman laser probing subsurface within the TPE, rather than Raman scattering from the outermost electrode surface. The similarities between the untreated sample and other treatments seems to support this hypothesis. It is also possible that graphite particles are not changing in a sufficiently large enough quantity as to largely affect the Raman signal. A combination of these two points is also quite logical.

The Lorentzian peak fitting of the spectra can be used to elucidate small changes. The D/G peak intensity ratio can be used to gauge the amount of disorder in a graphite sample.[69] Related to the amount of disorder is the crystallite domain, and a general equation based on the D/G ratio can be used to estimate the crystallite domain size (eq 2 in the Materials and Methods).[70] The calculated domain sizes are listed in Figure 7 above the spectra and indicate there is a slightly larger crystallite domain in the untreated and sanded samples, with polishing having the smallest crystallite domain. A similar trend was seen with the 20 μm particles-based TPE (Figure S9). The $\leq$500 nm TPE had essentially no crystallite domain size changes among surface treatments. The smaller domain size, seen with the 11 and 20 μm particles is reasonable since plasma treatment and polishing are secondary, coming after an initial sanding step. The values in Figure 7 imply that the changes in crystallite domain size are small, but give evidence toward polishing and plasma treatment chemically altering the carbon particles or removing larger particles. The plasma-treated TPE had the largest standard deviation associated with the crystallite domain (21 nm), as well as the largest relative standard deviation (28%). The larger standard deviation would suggest a more heterogeneous surface, qualitatively consistent with the SEM images. Finally, while it is clear that the surface treatments can induce some effect upon the carbon at the TPE surface, at this time, relating these differences to changes in the electrochemistry is not straightforward.

■ CONCLUSION

The work presented highlights the fabrication of solvent processed thermoplastic electrodes and their resulting electrochemical, physical and Raman characterization. The unique processing method enabled an electrode material which demonstrates both easy fabrication, high conductivity, and excellent electrochemistry. Through judicious selection of the particle type, particle-to-binder ratio, and surface treatment, the electrochemical and physical properties can be varied greatly. The electrode material also adds the ability to create micrometer-sized features using an array of common fabrication methods, including embossing. Of significant importance is that these new low-cost graphite electrodes can realize high electrochemical activity when properly activated, similar to that of more exotic carbons like carbon nanotubes, graphene, or HOPG.

■ ASSOCIATED CONTENT

Supporting Information

The Supporting Information is available free of charge on the ACS Publications website at DOI: 10.1021/jacs.7b06173.

DOI: 10.1021/jacs.7b06173
J. Am. Chem. Soc. 2017, 139, 12623−12631

Additional information regarding the impact of particle size and variations in processing methods, including eqs S1 and S2, Figures S1−S9, and Table S1 (PDF)

AUTHOR INFORMATION

Corresponding Author

*chuck.henry@colostate.edu

ORCID

Charles S. Henry: 0000-0002-8671-7728

Notes

The authors declare no competing financial interest.

ACKNOWLEDGMENTS

The authors thank the National Institute of Occupational Safety and Health for financial support through grant R01OH010662. This material is based upon work supported by the National Science Foundation under Grant No. 1710222. Additional support was provided by Colorado State University. Special thanks to Dr. Patrick McCurdy for acquiring the SEM images, and Eka Noviana for construction of the band electrodes in Figure 1B.

REFERENCES

(1) McCreery, R. L. *Chem. Rev.* **2008**, *108*, 2646−2687.
(2) Goriparti, S.; Miele, E.; De Angelis, F.; Di Fabrizio, E.; Proietti Zaccaria, R.; Capiglia, C. *J. Power Sources* **2014**, *257*, 421−443.
(3) Antunes, R. A.; de Oliveira, M. C. L.; Ett, G.; Ett, V. *J. Power Sources* **2011**, *196*, 2945−2961.
(4) Mussa, Z. H.; Othman, M. R.; Abdullah, M. P. *J. Braz. Chem. Soc.* **2015**, *26*, 939−948.
(5) Duan, F.; Li, Y.; Cao, H.; Wang, Y.; Crittenden, J. C.; Zhang, Y. *Chemosphere* **2015**, *125*, 205−211.
(6) Li, X.; Wei, B. *Nano Energy* **2013**, *2*, 159−173.
(7) Lee, B.-L. *Polym. Eng. Sci.* **1992**, *32*, 36−42.
(8) Randviir, E. P.; Brownson, D. A. C.; Metters, J. P.; Kadara, R. O.; Banks, C. E. *Phys. Chem. Chem. Phys.* **2014**, *16*, 4598−4611.
(9) Hayat, A.; Marty, J. L. *Sensors* **2014**, *14*, 10432−10453.
(10) Adams, R. N. *Anal. Chem.* **1958**, *30*, 1576−1576.
(11) Wang, J.; Naser, N. *Anal. Chim. Acta* **1995**, *316*, 253−259.
(12) Opallo, M.; Lesniewski, A. *J. Electroanal. Chem.* **2011**, *656*, 2−16.
(13) Henriques, H. P.; Fogg, A. G. *Analyst* **1984**, *109*, 1195−1199.
(14) Clem, R. G.; Sciamanna, A. F. *Anal. Chem.* **1975**, *47*, 276−280.
(15) McLaren, K. G.; Batley, G. E. *J. Electroanal. Chem. Interfacial Electrochem.* **1977**, *79*, 169−178.
(16) Yao, X.; Xu, X.; Yang, P.; Chen, G. *Electrophoresis* **2006**, *27*, 3233−3242.
(17) Klatt, L. N.; Connell, D. R.; Adams, R. E.; Honigberg, I. L.; Price, J. C. *Anal. Chem.* **1975**, *47*, 2470−2472.
(18) Wang, J.; Musameh, M. *Anal. Chem.* **2003**, *75*, 2075−2079.
(19) Mascini, M.; Liberti, A. *Anal. Chim. Acta* **1970**, *51*, 231−237.
(20) Liberti, A.; Morgia, C.; Mascini, M. *Anal. Chim. Acta* **1985**, *173*, 157−164.
(21) Zhong, S.; Kazacos, M.; Burford, R. P.; Skyllas-Kazacos, M. *J. Power Sources* **1991**, *36*, 29−43.
(22) Becker, H.; Locascio, L. E. *Talanta* **2002**, *56*, 267−287.
(23) Mascini, M.; Liberti, A. *Anal. Chim. Acta* **1969**, *47*, 339−345.
(24) Kauffmann, J. M.; Laudet, A.; Patriarche, G. J. *Anal. Lett.* **1982**, *15*, 763−774.
(25) Yao, X.; Wu, H.; Wang, J.; Qu, S.; Chen, G. *Chem. - Eur. J.* **2007**, *13*, 846−853.
(26) Regel, A.; Lunte, S. *Electrophoresis* **2013**, *34*, 2101−2106.
(27) Yang, K. L.; Yiacoumi, S.; Tsouris, C. *J. Electroanal. Chem.* **2003**, *540*, 159−167.
(28) Anandan, V.; Rao, Y. L.; Zhang, G. *Int. J. Nanomed.* **2006**, *1*, 73−79.
(29) Anandan, V.; Yang, X.; Kim, E.; Rao, Y. L.; Zhang, G. *J. Biol. Eng.* **2007**, *1*, 5−5.
(30) Suherman, H.; Sahari, J.; Sulong, A. B. *Adv. Mater. Res.* **2011**, *265*, 559−564.
(31) Pham, V. H.; Dang, T. T.; Hur, S. H.; Kim, E. J.; Chung, J. S. *ACS Appl. Mater. Interfaces* **2012**, *4*, 2630−2636.
(32) Wu, C.; Huang, X.; Wang, G.; Lv, L.; Chen, G.; Li, G.; Jiang, P. *Adv. Funct. Mater.* **2013**, *23*, 506−513.
(33) Arenhart, R. G.; Barra, G. M. O.; Fernandes, C. P. *Polym. Compos.* **2016**, *37*, 61−69.
(34) Pandolfo, A. G.; Wilson, G. J.; Huynh, T. D.; Hollenkamp, A. F. *Fuel Cells* **2010**, *10*, 856−864.
(35) Bârsan, O. A.; Hoffmann, G. G.; van der Ven, L. G. J.; de With, G. *Adv. Funct. Mater.* **2016**, *26*, 4377−4385.
(36) Deng, H.; Lin, L.; Ji, M.; Zhang, S.; Yang, M.; Fu, Q. *Prog. Polym. Sci.* **2014**, *39*, 627−655.
(37) Gautam, R. K.; Kar, K. K. *Fuel Cells* **2016**, *16*, 179−192.
(38) Balazs, A. C.; Emrick, T.; Russell, T. P. *Science* **2006**, *314*, 1107−1110.
(39) Chen, P.; McCreery, R. L. *Anal. Chem.* **1996**, *68*, 3958−3965.
(40) DuVall, S. H.; McCreery, R. L. *Anal. Chem.* **1999**, *71*, 4594−4602.
(41) McDermott, C. A.; Kneten, K. R.; McCreery, R. L. *J. Electrochem. Soc.* **1993**, *140*, 2593−2599.
(42) Kadara, R. O.; Jenkinson, N.; Banks, C. E. *Sens. Actuators, B* **2009**, *138*, 556−562.
(43) Kozbial, A.; Zhou, F.; Li, Z.; Liu, H.; Li, L. *Acc. Chem. Res.* **2016**, *49*, 2765−2773.
(44) Hallam, P. M.; Banks, C. E. *Electrochem. Commun.* **2011**, *13*, 8−11.
(45) O'Hare, D.; Macpherson, J. V.; Willows, A. *Electrochem. Commun.* **2002**, *4*, 245−250.
(46) Guo, S.-X.; Zhao, S.-F.; Bond, A. M.; Zhang, J. *Langmuir* **2012**, *28*, 5275−5285.
(47) Streeter, I.; Wildgoose, G. G.; Shao, L.; Compton, R. G. *Sens. Actuators, B* **2008**, *133*, 462−466.
(48) Cvelbar, U.; Markoli, B.; Poberaj, I.; Zalar, A.; Kosec, L.; Spaić, S. *Appl. Surf. Sci.* **2006**, *253*, 1861−1865.
(49) Huang, J. Y. *Acta Mater.* **1999**, *47*, 1801−1808.
(50) Chethana, B. K.; Arthoba Naik, Y. *Anal. Methods* **2012**, *4*, 3754−3759.
(51) Sudhakara Prasad, K.; Muthuraman, G.; Zen, J.-M. *Electrochem. Commun.* **2008**, *10*, 559−563.
(52) Falat, L.; Cheng, H. Y. *Anal. Chem.* **1982**, *54*, 2108−2111.
(53) Zhu, S.; Li, H.; Niu, W.; Xu, G. *Biosens. Bioelectron.* **2009**, *25*, 940−943.
(54) Raoof, J. B.; Ojani, R.; Baghayeri, M. *Anal. Methods* **2011**, *3*, 2367−2373.
(55) Kachoosangi, R. T.; Banks, C. E.; Compton, R. G. *Electroanalysis* **2006**, *18*, 741−747.
(56) Wantz, F.; Banks, C. E.; Compton, R. G. *Electroanalysis* **2005**, *17*, 1529−1533.
(57) Hadi, M.; Rouhollahi, A. *Anal. Chim. Acta* **2012**, *721*, 55−60.
(58) Brownson, D. A. C.; Foster, C. W.; Banks, C. E. *Analyst* **2012**, *137*, 1815−1823.
(59) Patel, A. N.; Tan, S.-y.; Miller, T. S.; Macpherson, J. V.; Unwin, P. R. *Anal. Chem.* **2013**, *85*, 11755−11764.
(60) Wang, J.; Walcarius, A. *J. Electroanal. Chem.* **1996**, *407*, 183−187.
(61) Yi, M.; Shen, Z. *J. Mater. Chem. A* **2015**, *3*, 11700−11715.
(62) Malekpour, H.; Chang, K. H.; Chen, J. C.; Lu, C. Y.; Nika, D. L.; Novoselov, K. S.; Balandin, A. A. *Nano Lett.* **2014**, *14*, 5155−5161.
(63) Couzi, M.; Bruneel, J.-L.; Talaga, D.; Bokobza, L. *Carbon* **2016**, *107*, 388−394.
(64) Cançado, L. G.; Takai, K.; Enoki, T.; Endo, M.; Kim, Y. A.; Mizusaki, H.; Speziali, N. L.; Jorio, A.; Pimenta, M. A. *Carbon* **2008**, *46*, 272−275.
(65) Dresselhaus, M. S.; Jorio, A.; Cançado, L. G.; Dresselhaus, G.; Saito, R. In *Raman Spectroscopy: Characterization of Edges, Defects, and*

DOI: 10.1021/jacs.7b06173
J. Am. Chem. Soc. 2017, 139, 12623−12631

the Fermi Energy of Graphene and sp 2 Carbons; Raza, H., Ed.; Springer: Berlin/Heidelberg, 2012; pp 15−55.
(66) Schäfer, H.; Hess, C.; Tobergte, H.; Volf, A.; Ichilmann, S.; Eickmeier, H.; Voss, B.; Kashaev, N.; Nordmann, J.; Akram, W.; Hartmann-Azanza, B.; Steinhart, M. *Small* **2015**, *11*, 931−935.
(67) Yue, X.; Wang, H.; Wang, S.; Zhang, F.; Zhang, R. *J. Alloys Compd.* **2010**, *505*, 286−290.
(68) Pattammattel, A.; Kumar, C. V. *Adv. Funct. Mater.* **2015**, *25*, 7088−7098.
(69) Jorio, A.; Ferreira, E. H. M.; Moutinho, M. V. O.; Stavale, F.; Achete, C. A.; Capaz, R. B. *Phys. Status Solidi B* **2010**, *247*, 2980−2982.
(70) Cançado, L. G.; Takai, K.; Enoki, T.; Endo, M.; Kim, Y. A.; Mizusaki, H.; Jorio, A.; Coelho, L. N.; Magalhães-Paniago, R.; Pimenta, M. A. *Appl. Phys. Lett.* **2006**, *88*, 163106.

DOI: 10.1021/jacs.7b06173
J. Am. Chem. Soc. 2017, 139, 12623−12631